applied sciences

MDPI

Article

Vibration Analysis of Non-Uniform Rods Considering Lateral Inertia Effects Under Ultrasonic Excitation

Jie Wan, Yuehang Zhang, Chengpeng Chu, Qiyu Gao, Guangming Xing, Kaiming Sun, Yuanjing Mu, Qi Li, Ming Li and Yan Zhang *

Department of Intelligent Manufacturing Engineering, School of Mechanical and Vehicle Engineering, Changchun University, Changchun 130022, China
* Correspondence: zhangy198705@163.com

Abstract

Non-uniform rods are widely present in ultrasonic vibration systems, and the accuracy of their resonance design significantly impacts system performance. Traditional design methods often treat non-uniform rods as one-dimensional members, neglecting the influence of lateral inertia, which results in lower resonance design accuracy. This paper establishes a vibration model for non-uniform rods under ultrasonic excitation that accounts for lateral inertia effects. Subsequently, the natural frequencies and mode shapes of the rod are obtained using the transfer matrix method. The modal superposition method is then employed to derive the internal displacement distribution function and stress distribution function of the rod. The validation of the tapered rod and the ultrasonic fatigue specimen demonstrates that the proposed method is closer to the Finite Element Method (FEM) results than the traditional method. The results show that the relative deviation between the resonant length of the tapered rod and the FEM calculation is less than 0.16%, and the harmonic response analysis results of the two are also in good agreement; the relative deviation between the first-order natural frequency of the ultrasonic fatigue specimen and the FEM calculation is less than 0.315%, and the predicted maximum stress is highly consistent with the FEM. The research findings presented herein can serve as a universal methodology for resonance design and performance evaluation of longitudinal vibration components in ultrasonic vibration systems.

Keywords: non-uniform rods; ultrasonic excitation; lateral inertia effect; transfer matrix method; vibration analysis

Check for updates

Academic Editor: Junhong Park

Received: 30 March 2026
Revised: 27 April 2026
Accepted: 30 April 2026
Published: 4 May 2026

Copyright: © 2026 by the authors. Licensee MDPI, Basel, Switzerland. This article is an open access article distributed under the terms and conditions of the Creative Commons Attribution (CC BY) license.

1. Introduction

Non-uniform rods are widely used in applications such as ultrasonic machining [1–3], ultrasonic welding [4–6], and ultrasonic fatigue [7–9] due to their excellent performance in vibrational energy transfer and amplitude regulation. In these applications, non-uniform rods primarily function as ultrasonic horn amplifiers and ultrasonic fatigue specimens, operating in a resonant state. Ultrasonic horn amplifiers primarily amplify amplitude and concentrate energy within ultrasonic vibration systems. Their design precision directly impacts the stable and accurate output of amplitude, thereby influencing processing quality. Under ultrasonic excitation, ultrasonic fatigue specimens [10] generate high-frequency alternating stress (strain) fields internally, with the maximum stress occurring at the specimen's mid-section (the intended fracture location). Given that ultrasonic fatigue specimens operate in resonance, the design precision of their resonant dimensions directly influences the location and magnitude

of maximum stress, thereby affecting the reliability of fatigue test data. Therefore, conducting vibration analysis research on non-uniform rods under ultrasonic excitation, exploring new methods for resonant design of non-uniform rods, and achieving rapid, precise design of resonant dimensions all hold significant importance.

Considering that the resonance design of ultrasonic fatigue specimens is essentially a special case of ultrasonic horn design, where the fatigue specimen is fundamentally a mirrored combination of two quarter-wavelength horns, the following discussion will focus solely on the current state of research regarding ultrasonic horn design methodologies. Traditional ultrasonic horn designs typically treat them as one-dimensional non-uniform rods undergoing longitudinal vibration, neglecting the influence of transverse (radial) vibration. If an ultrasonic horn possesses special cross-sectional profiles such as exponential, catenary, tapered, stepped, or wedge shapes, its wave equation can yield analytical solutions under simple boundary conditions. Consequently, performance parameters like resonant length, displacement nodes, shape factor, and amplification coefficient can be directly calculated [11]. However, this traditional analytical method is limited to single-element amplifiers and is not applicable to amplifiers with complex outer contours or cross-sections. To design such amplifiers, the equivalent circuit method [12,13] and the transfer matrix method [14] have been applied. Both methods involve segmenting the ultrasonic horn, performing analytical solutions for each segment, and then combining them under inter-segment continuity conditions to obtain the equivalent circuit or overall transfer matrix for the entire ultrasonic horn, thereby enabling its design. None of the aforementioned ultrasonic horn design methods consider the influence of lateral vibrations, which can lead to significant design deviations for ultrasonic horns with radial dimensions exceeding 1/4 wavelength [11]. Given that analytical solutions for three-dimensional vibration theory considering lateral coupling vibrations generally do not exist, the apparent elasticity method was proposed and applied to the design of ultrasonic horn [15,16]. This method considers only tensile and compressive deformations, disregarding shear deformation. It describes vibrations in different directions using distinct apparent elastic constants, then calculates resonant frequencies using elastic stress ratios (i.e., coupling parameters) in each direction. This method has also been applied to the design of connectors and amplitude-modulating rods incorporating material damping, with design accuracy validated through finite element simulations and experiments [17]. With advances in computing technology, the finite element method (FEM), as an alternative approach for solving three-dimensional vibrations, has gained increasing application in designing irregular, non-analytically solvable horn structures due to its versatility and intuitiveness. Examples include horns for ultrasonic welding [5] and ultrasonic machining [2]. However, among these three-dimensional vibrations analysis-based ultrasonic horn design methods, the apparent elasticity method suffers from computational complexity and inconvenience for engineering implementation. Meanwhile, the FEM requires iterative calculations in resonant design where natural frequencies are known, resulting in low computational efficiency.

In summary, although the traditional analytical method, equivalent circuit method, and transfer matrix method are widely used in non-uniform rod design, they are mostly limited by one-dimensional theory and ignore the influence of lateral vibration, leading to large design deviations for components with large radial dimensions. Further, while the apparent elasticity method and finite element method can account for three-dimensional effects, they face the limitations of tedious calculation processes and low efficiency in reverse resonant design. Aiming at this current situation, this paper introduces the transfer matrix method [18] (TMM), which possesses high efficiency and universal characteristics, into the vibration analysis of non-uniform rods. By constructing a dynamic model considering lateral inertia correction, a general analysis method combining high computational accuracy

and engineering design efficiency is proposed to fill the research gap in balancing lateral effects and design efficiency for complex non-uniform rods.

For the vibration analysis of non-uniform rods under ultrasonic excitation, this paper is organized as follows: Section 2 establishes a vibration model for non-uniform rods under ultrasonic excitation, incorporating the influence of lateral inertia and material damping through the introduction of the Kelvin model. Section 3 performs free vibration analysis by approximating the non-uniform rod as an equivalent rod composed of uniform cross-section rods and applying the transfer matrix method. Section 4 first derives the orthogonality conditions for the natural mode functions of the non-uniform rod. Based on these conditions, steady-state response analysis is performed using the modal superposition method. Section 5 validates the accuracy of the proposed method through typical numerical examples and practical applications. Section 6 presents concluding remarks.

2. Dynamic Model

Traditional one-dimensional longitudinal wave theory assumes that the cross-sectional area of a rod remains unchanged before and after deformation. However, in reality, the particles in the rod exhibit lateral inertia. The mechanism of the lateral inertia effect originates from the Poisson effect of the material. Under axial dynamic loading, the lateral contraction or expansion of the specimen generates corresponding lateral kinetic energy, leading to differences in the phase velocities of harmonics at different frequencies and causing geometric dispersion. This, in turn, invalidates the traditional plane section assumption and results in a non-uniform stress distribution across the cross-section. As the ratio of the rod diameter to the wavelength increases, the influence of this lateral inertia effect becomes more significant [19]. Therefore, incorporating lateral inertia into the free/forced vibration models of non-uniform rods enhances the accuracy of vibration analysis results. This section establishes a vibration model for non-uniform rods under ultrasonic excitation, accounting for the influence of lateral inertia.

Components within ultrasonic vibration systems are typically connected using bolts. To prevent fatigue failure of connecting bolts due to excessive stress during operation, it is essential to minimize stress at the connection points of ultrasonic components. Considering that ultrasonic components operate in a resonant state, the longitudinal vibration amplitude at their connection points should be maximized under free vibration conditions. This corresponds to the boundary conditions at both ends of the non-uniform rod being in a free state. Therefore, ultrasonic excitation is typically regarded as a concentrated excitation force applied at the ends [20]. Figure 1 illustrates the stress analysis diagram of the non-uniform rod and its microelements under ultrasonic excitation.

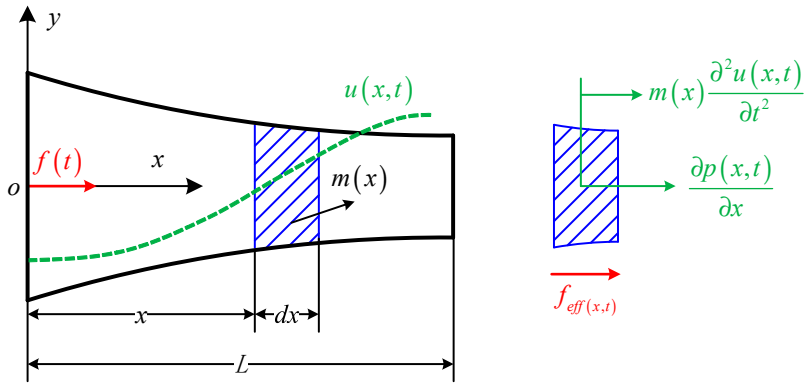


Figure 1. Force analysis of a damped non-uniform rod and its microelements under ultrasonic excitation.

When the ultrasonic excitation is regarded as a concentrated excitation force, it can be expressed in the following distributed force form [20]:

$$f_{eff}(x,t) = f(t)\delta(x) = P_0\delta(x)cos(\Omega t) \tag{1}$$

where $\delta(x)$ is the unit impulse function, P_0 is the amplitude of the concentrated excitation force, and Ω is the circular excitation frequency.

By performing a force analysis on the microelement and applying Newton's second law, the governing equation is obtained as follows:

$$m(x)\frac{\partial^2 u(x,t)}{\partial t^2} = \frac{\partial p(x,t)}{\partial x} + f_{eff}(x,t) \tag{2}$$

where $m(x) = \rho(x)S(x)$ is the mass of the microelement, $\rho(x)$ is the density of the rod, $S(x)$ is the cross-sectional area of the microelement, $u(x,t)$ is the longitudinal displacement, $p(x,t) = [\sigma(x,t) + \sigma_D(x,t)]S(x)$ is the internal axial force, $\sigma(x,t)$ is the longitudinal stress, and $\sigma_D(x,t)$ is the damping term of the stress.

When considering the effect of lateral inertia, the expression for the longitudinal stress in the microelement can be written as [19]:

$$\sigma(x,t) = E(x)\frac{\partial u(x,t)}{\partial x} + \rho(x)v^2r^2\frac{\partial^3 u(x,t)}{\partial x \partial t^2} \tag{3}$$

where $E(x)$ is the elastic modulus of the rod material, v is Poisson's ratio of the rod material, and r is the radius of gyration of the cross-section about the x-axis. Its expression is:

$$r = \sqrt{\frac{1}{S(x)}\iint_0^{S(x)} (y^2 + z^2)dydz} \tag{4}$$

Given that ultrasonic components in longitudinal vibration have a small contact area with the external air, the viscous damping caused by external air is neglected in the established forced vibration model, and only the influence of material damping is considered. The Kelvin–Voigt model is a commonly used material damping model [21]. This paper introduces it into the established model. The damping term of the stress can be expressed as:

$$\sigma_D(x,t) = \beta E(x)\frac{\partial^2 u(x,t)}{\partial x \partial t} \tag{5}$$

where β is the material damping coefficient.

Substituting Equations (1), (3) and (5) into Equation (2), the longitudinal vibration model of a damped non-uniform rod under ultrasonic excitation is obtained as:

$$m(x)\frac{\partial^2 u}{\partial t^2} - \frac{\partial}{\partial x}\left[m(x)\nu^2 r^2\frac{\partial^3 u}{\partial x \partial t^2}\right] - \frac{\partial}{\partial x}\left[E(x)S(x)\left(\frac{\partial u}{\partial x} + \beta\frac{\partial^2 u}{\partial x \partial t}\right)\right] = P_0\delta(x)cos(\Omega t) \tag{6}$$

where u is the shorthand form of $u(x,t)$, and the boundary conditions for the above equation are:

$$\sigma(x,t)|_{x=0} = \sigma(x,t)|_{x=L} = 0 \tag{7}$$

3. Free Vibration

In this section, the method of separated variables and TMM are introduced to perform free vibration analysis on the damped non-uniform rod, thereby obtaining its natural frequencies and mode shapes.

Under free vibration conditions (i.e., $P_0 = 0$), the free vibration model of a damped non-uniform rod considering lateral inertia effects can be expressed as:

$$m(x)\frac{\partial^2 u}{\partial t^2} - \frac{\partial}{\partial x}\left[m(x)v^2r^2\frac{\partial^3 u}{\partial x \partial t^2}\right] - \frac{\partial}{\partial x}\left[E(x)S(x)\left(\frac{\partial u}{\partial x} + \beta\frac{\partial^2 u}{\partial x \partial t}\right)\right] = 0 \tag{8}$$

By introducing the method of separation of variables to solve the above partial differential equation. The longitudinal displacement of the rod can be expressed as [22]:

$$u(x,t) = U(x)T(t) \tag{9}$$

where $U(x)$ is the spatial function of the longitudinal displacement, and $T(t)$ is the temporal function.

Substituting the above equation into Equation (8), and after simplification, ordinary differential equations for the spatial function and the temporal function are obtained respectively:

$$\frac{d}{dx}\left[E(x)S(x)\frac{dU(x)}{dx}\right] - \omega^2\frac{d}{dx}\left[v^2r^2m(x)\frac{dU(x)}{dx}\right] + \omega^2 m(x)U(x) = 0 \tag{10}$$

$$\frac{d^2}{dt^2}T(t) + \beta\omega^2\frac{d}{dt}T(t) + \omega^2 T(t) = 0 \tag{11}$$

where ω is the natural frequency of the longitudinal vibration of the non-uniform rod.

By solving the differential equations involving spatial functions under the boundary conditions of the non-uniform rod, the natural frequencies and mode shapes of the rod can be obtained. To solve these differential equations, the TMM is introduced, dividing the non-uniform rod into N uniform segments, as shown in Figure 2:

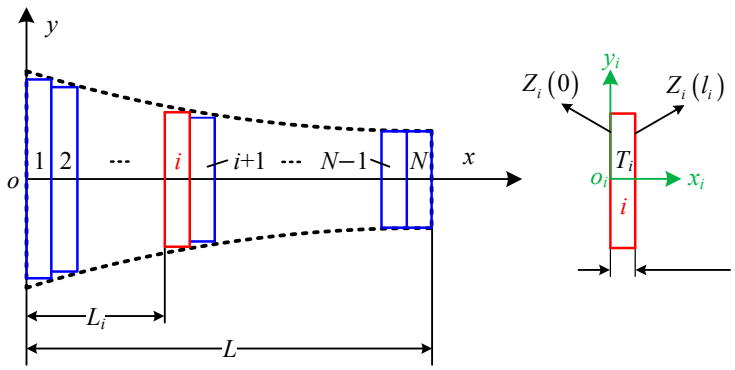


Figure 2. Schematic diagram of the non-uniform rod after equal division and its elements.

For the i-th uniform TMM element, Equation (10) can be rewritten as:

$$\frac{d^2U_{d,i}(x_i)}{dx_i^2} + \frac{\rho_i\omega^2}{E_i}U_{d,i}(x_i) = 0 \tag{12}$$

where $x_i = x - L_i$ is the axial coordinate in the element coordinate system $oixiyi$, $U_{d,i}(x_i)$ is the spatial function of the longitudinal displacement for the i-th element; ρ_i is the density of the i-th element; E_i is the equivalent stiffness of the i-th element considering lateral inertia effects, expressed as:

$$E_i = E_{d,i} - \rho_i\omega^2v^2r_i^2 \tag{13}$$

where $E_{d,i}$ and r_i are the elastic modulus and the radius of gyration of the i-th element, respectively. Refer to Equation (4) for the expression of the radius of gyration.

Let $k_i = \omega / \sqrt{E_i / \rho_i}$; the general solution form of Equation (12) can be expressed as:

$$U_{d,i}(x_i) = D_{1,i}\cos(k_i x_i) + D_{2,i} sin(k_i x_i) \tag{14}$$

Furthermore, combining Equations (3), (5), (9) and (11), the spatial function for the longitudinal stress distribution in the i-th element when considering lateral inertia effects:

$$\sigma_i(x_i) = E_i \frac{dU_{d,i}(x_i)}{dx_i} \tag{15}$$

Substituting Equation (14) into the above equation yields the spatial function of the internal axial force for the i-th element:

$$P_{d,i}(x_i) = \sigma_i(x_i) S_i = E_i k_i S_i [-D_{1,i}\sin(k_i x_i) + D_{2,i} cos(k_i x_i)] \tag{16}$$

where S_i is the cross-sectional area of the i-th element.

According to Equations (14) and (16), the spatial functions of the longitudinal displacement and internal axial force for the i-th element in the longitudinally vibrating rod can be expressed as:

$$\mathbf{Z}_i(x_i) = \mathbf{\Gamma}_i(x_i)\mathbf{D}_i \tag{17}$$

where

$$\mathbf{Z}_i(x_i) = \begin{bmatrix} U_{d,i}(x_i) & P_{d,i}(x_i) \end{bmatrix}^T \tag{18a}$$

$$\mathbf{D}_i = \begin{bmatrix} D_{1,i} & D_{2,i} \end{bmatrix}^T \tag{18b}$$

$$\mathbf{\Gamma}_i(x_i) = \begin{bmatrix} \cos(k_i x_i) & sin(k_i x_i) \\ -E_i k_i S_i \sin(k_i x_i) & E_i k_i S_i cos(k_i x_i) \end{bmatrix} \tag{18c}$$

Correspondingly, the undetermined coefficient matrices at $x_i = 0$ and $x_i = l_i = L/N$ can be expressed as:

$$\mathbf{D}_i = \mathbf{\Gamma}_i^{-1}(0)\mathbf{Z}_i(0) \tag{19a}$$

$$\mathbf{D}_i = \mathbf{\Gamma}_i^{-1}(l_i)\mathbf{Z}_i(l_i) \tag{19b}$$

Based on the above two equations, the transfer equation for the i-th element can be derived:

$$\mathbf{Z}_i(l_i) = \mathbf{\Gamma}_i(l_i)\mathbf{\Gamma}_i^{-1}(0)\mathbf{Z}_i(0) \tag{20}$$

Therefore, the transfer relation between the state vectors at the two ends of the i-th element is [18]

$$\mathbf{Z}_i(l_i) = \mathbf{T}_i\mathbf{Z}_i(0) \tag{21}$$

where $\mathbf{T}_i$ is the transfer matrix of the i-th element of the rod, expressed as:

$$\mathbf{T}_i = \mathbf{\Gamma}_i(l_i)\mathbf{\Gamma}_i^{-1}(0) \tag{22}$$

Correspondingly, the transfer relation for the state vectors at the two ends of the (i + 1)-th element can be expressed as:

$$\mathbf{Z}_{i+1}(l_{i+1}) = \mathbf{T}_{i+1}\mathbf{Z}_{i+1}(0) \tag{23}$$

According to the displacement continuity and force equilibrium conditions between the i-th and (i + 1)-th elements, we have:

$$\mathbf{Z}_i(l_i) = \mathbf{Z}_{i+1}(0) \tag{24}$$

Therefore, the overall transfer equation for the two ends of the rod is:

$$\mathbf{Z}_N(l_N) = \mathbf{G}\mathbf{Z}_1(0) \tag{25}$$

where G is the overall transfer matrix of the rod, expressed as:

$$\mathbf{G} = \prod_{i=1}^{N} \mathbf{T}_i \tag{26}$$

Introducing the boundary conditions for the longitudinally vibrating non-uniform rod, its frequency equation can be expressed as:

$$\begin{vmatrix} \mathbf{B}_0 \\ \mathbf{B}_L\mathbf{G} \end{vmatrix} = 0 \tag{27}$$

For a longitudinally vibrating rod, the simple boundary condition matrices $\mathbf{B}_0$ and $\mathbf{B}_L$ are shown in Table 1:

Table 1. Simple boundary condition matrices for a longitudinally vibrating rod.

	Free	**Fixed**
$\mathbf{B}_0$, $\mathbf{B}_L$	$\begin{bmatrix} 0 & 1 \end{bmatrix}$	$\begin{bmatrix} 1 & 0 \end{bmatrix}$

Under ultrasonic excitation, the rod is free at both ends, so its simple boundary condition matrices $\mathbf{B}_0$ and $\mathbf{B}_L$ are:

$$\mathbf{B}_0 = \mathbf{B}_L = \begin{bmatrix} 0 & 1 \end{bmatrix} \tag{28}$$

The frequency equation for the longitudinally vibrating non-uniform rod under free boundary conditions can be obtained from Equation (27). Given the dimensions of the non-uniform rod, its natural frequencies ω_n of different orders can be obtained from the frequency equation. Given that $k_i = \omega_n / \sqrt{E_i/\rho_i}$, the matrices $\mathbf{\Gamma}_i(0)$ and $\mathbf{\Gamma}_i(l_i)$ can be determined. Furthermore, the boundary conditions of the non-uniform rod determine the state vector $\mathbf{Z}_1(0)$ of the initial element. Substituting this into Equation (19a), the undetermined coefficient matrix for the initial element is given by

$$\mathbf{D}_1 = \mathbf{\Gamma}_1^{-1}(0)\mathbf{Z}_1(0) \tag{29}$$

Combining Equations (19), (20), (22) and (24), the undetermined coefficient matrix for the i-th element is obtained as:

$$\mathbf{D}_i = \mathbf{\Gamma}_i^{-1}(0)\prod_{r=1}^{i-1}\mathbf{T}_r\mathbf{Z}_1(0),\ i > 1 \tag{30}$$

Substituting Equations (29) and (30) into Equation (17), the mode shape function $U_{\mathrm{d},i}(x_i)$ for the i-th element corresponding to ω_n is obtained. Therefore, the n-th order mode shape function of the non-uniform rod can be expressed as:

$$U_n(x) = U_{\mathrm{d},i}(x - L_i),\ x \in [L_i,\ L_i + l_i] \tag{31}$$

4. Steady-State Forced Vibration

This paper employs the modal superposition method to solve the steady-state response of the damped non-uniform rod. When applying this method, in addition to obtaining the natural frequencies and mode shape functions of the non-uniform rod under free boundary conditions, it is also necessary to ensure that its mode shape functions satisfy the orthogonality conditions.

Specifically, the orthogonality conditions for the mode shape functions of the non-uniform rod need to be derived considering the influence of lateral inertia.

4.1. Orthogonality Conditions

The n-th order mode shape function of the non-uniform rod satisfies Equation (10), leading to the following relationship containing $U_n(x)$:

$$\omega_n^2 \frac{d}{dx}\left[\nu^2 r^2 m(x)\frac{dU_n}{dx}\right] - \omega_n^2 m(x)U_n = \frac{d}{dx}\left[E(x)S(x)\frac{dU_n}{dx}\right] \tag{32}$$

where U_n is the shorthand form of $U_n(x)$.

Multiplying the above equation by the m-th order mode shape function $U_m(x)$, integrating along x, applying integration by parts, and then combining this with the free boundary conditions at the rod ends under free vibration, we simplify to obtain:

$$\omega_n^2 \int_0^L m(x)U_m U_n dx + \omega_n^2 \int_0^L \nu^2 r^2 m(x)\frac{dU_m}{dx}\frac{dU_n}{dx}dx = \int_0^L E(x)S(x)\frac{dU_m}{dx}\frac{dU_n}{dx}dx \tag{33}$$

Similarly, the m-th order mode shape function satisfies the following relationship:

$$\omega_m^2 \int_0^L m(x)U_m U_n dx + \omega_m^2 \int_0^L \nu^2 r^2 m(x)\frac{dU_m}{dx}\frac{dU_n}{dx}dx = \int_0^L E(x)S(x)\frac{dU_m}{dx}\frac{dU_n}{dx}dx \tag{34}$$

Subtracting the two equations above and incorporating Equation (33), we obtain the following simplified expression:

$$\frac{\omega_n^2 - \omega_m^2}{\omega_n^2}\int_0^L E(x)S(x)\frac{dU_n}{dx}dU_m = 0 \tag{35}$$

By performing integration by parts to the above equation and considering the free boundary conditions at the rod ends, we obtain that:

$$\int_0^L E(x)S(x)\frac{dU_n}{dx}dU_m = -\int_0^L U_m \frac{d}{dx}\left[E(x)S(x)\frac{dU_n}{dx}\right]dx \tag{36}$$

Substituting the above equation into Equation (35), the orthogonality condition for the mode functions of a non-uniform rod under the influence of lateral inertia is given as:

$$\int_0^L U_m \frac{d}{dx}\left[E(x)S(x)\frac{dU_n}{dx}\right]dx = 0,\ \omega_n \neq \omega_m \tag{37}$$

4.2. Modal Superposition Method

The modal superposition method is a common approach for solving the steady-state response of a non-uniform rod. When applied to solve the vibrational differential equation of a damped non-uniform rod under ultrasonic excitation, the longitudinal displacement within the rod can be approximated as:

$$u(x,t) \approx \sum_{m=1}^{N_m} U_m(x)T_m(t) \tag{38}$$

Substituting Equation (38) into Equation (6) and considering Equation (10), we obtain the following expression:

$$\sum_{m=1}^{N_m} U_m(x)\frac{d}{dx}\left[E(x)S(x)\frac{dU_m(x)}{dx}\right]\left[\frac{d^2}{dt^2}T_m(t) + 2\xi_m\omega_m\frac{d}{dt}T_m(t) + \omega_m^2 T_m(t)\right] = -\omega_n^2 P_0\delta(x)cos(\Omega t) \tag{39}$$

where $\xi_m = \beta_m\omega_m/2$ is the m-th order modal damping ratio.

Given that the research focus consistently remains on the n-th mode shape, the m-th mode shape is switched back to the n-th mode shape to strictly maintain the consistency of the research object in the subsequent theoretical derivations.

Multiplying both sides of Equation (39) by the n-th order mode shape function $U_n(x)$ of the rod and integrating over the entire length, then applying Equation (37), gives:

$$\frac{d^2}{dt^2}T_n(t) + 2\xi_n\omega_n\frac{d}{dt}T_n(t) + \omega_n^2 T_n(t) = \frac{\omega_n^2}{K_n}P_0U_n(0)cos(\Omega t) \tag{40}$$

where K_n is the generalized stiffness of the rod in modal coordinates, expressed as:

$$K_n = -\int_0^L U_n(x)\frac{d}{dx}\left[E(x)S(x)\frac{dU_n(x)}{dx}\right]dx \tag{41}$$

According to Duhamel's integral, the steady-state solution of Equation (40) is:

$$T_n(t) = \frac{\omega_n^2}{K_n}P_0U_n(0)\frac{2\xi_n\Omega\omega_n}{\left(\Omega^2+\omega_n^2\right)^2 - (2\Omega\omega_d)^2}\cos(\Omega t - \theta_n) \tag{42}$$

where $\omega_d = \omega_n\sqrt{1-\xi_n^2}$, $\theta_n = arctan\frac{2\xi_n\Omega\omega_n}{\omega_n^2-\Omega^2}$.

Substituting the above into Equation (38), the steady-state response of the rod's vibrational displacement is obtained. However, the amplitude of the concentrated excitation force in the steady-state response function under ultrasonic excitation is unknown; this unknown parameter can be calculated from the measured amplitude at the rod end. Considering that longitudinal vibration ultrasonic components generally operate at their natural frequency (i.e., $\Omega = \omega_n$), the superposition term of the displacement distribution function for this component is dominated by the n-th order mode. Therefore, the displacement distribution function of the longitudinal vibration ultrasonic component can be approximated as:

$$u(x,t) = \frac{1}{2\xi_n K_n}P_0U_n(x)\sin(\omega_n t) \tag{43}$$

If the measured displacement amplitude at the end of the longitudinal vibration component (i.e., the rod end) is H_r and the mode shape function is normalized (i.e., $U_n(0) = 1$), the applied concentrated excitation force amplitude can be obtained from the above equation as:

$$P_0 = 2\xi_n K_n H_r \tag{44}$$

It can be seen from the equation that the amplitude of the concentrated excitation force corresponding to the ultrasonic excitation is related not only to the end amplitude of the excited ultrasonic component but also to the material damping. As the material damping increases, the required excitation force amplitude also increases. To reduce the load on the ultrasonic driving assembly, the excited ultrasonic component should be made of materials with low material damping. Taking ultrasonic horns as an example, the selected material generally requires low loss and high fatigue strength within the operating frequency range, such as titanium alloys, aluminum alloys, etc. [11].

Substituting Equation (44) into Equation (43), and then combining with Equation (3), the displacement distribution function and stress distribution function of the longitudinal vibration ultrasonic component when $\Omega = \omega_n$ are obtained as:

$$u(x,t) = H_rU_n(x)\sin(\omega_n t) \tag{45}$$

$$\sigma(x,t) = H_r\left[E(x) - \rho(x)v^2r^2\omega_n^2\right]\frac{dU_n(x)}{dx}sin(\omega_n t) \tag{46}$$

5. Verification and Application

In this section, the validity and accuracy of the established model and its computational method are verified through a typical non-uniform rod example (i.e., a tapered rod) and a typical application instance (i.e., an ultrasonic fatigue specimen). In the aforementioned examples, the proposed computational method is implemented using MATLAB (R2023b, MathWorks Inc., Natick, MA, USA) software, and the Finite Element Method (FEM) results are obtained using the commercial finite element software ANSYS (v15.0, ANSYS Inc., Canonsburg, PA, USA).

5.1. Verification: Tapered Rod

As a typical non-uniform rod, the tapered rod serves as a representative case study with universal applicability. This section takes the TC4 titanium alloy as the research object. To facilitate comparison with results in the literature, the material parameters of the rod do not vary along the axial direction and are specified as follows: E = 109 GPa, ρ = 4440 kg/m^3, Poisson's ratio is 0.3, and the damping ratio is 0.04. The dimensional parameters of the rod are shown in Figure 3, where R_1 = 16 mm, R_2 = 8 mm, L = 130 mm, and the radius at any point is given by $R(x) = R_1 - (R_1 - R_2)x/L$.

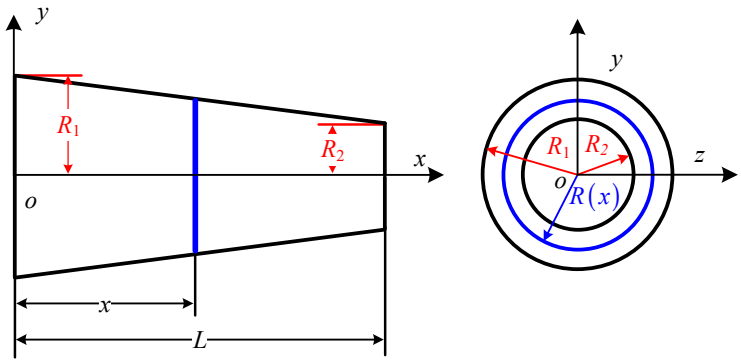


Figure 3. Schematic diagram of the tapered rod dimensions.

To verify the convergence of the algorithm proposed in the research, the proposed method was used to calculate the corresponding ω_1 and ω_2 when the number of segments N of the free-ended tapered rod changed from 1 to 50. To facilitate subsequent comparison with results from the literature, the calculated natural frequencies were normalized. The nth-order dimensionless natural frequency is expressed as [23]:

$$\Omega_n = \omega_n L \sqrt{\frac{\rho}{E}} \tag{47}$$

Furthermore, the mode shape functions $U_1(x)$ and $U_2(x)$ for the tapered rod were obtained for N = 1, N = 3, N = 20, and N = 50, as shown in Figures 4 and 5.

The curves in Figures 4 and 5 indicate that as the number of segments N increases, Ω_1 and Ω_2 tend toward stable values. Correspondingly, the mode functions also stabilize with increasing N. Similar to FEM, a larger number of elements implies that the interpolation functions within each element (i.e., the characteristic functions of elements in TMM) more closely approximate the actual mode shapes of non-uniform rods. Consequently, the natural frequencies derived from the boundary conditions become more accurate. However, as N increases, this improvement in computational accuracy becomes increasingly insignificant, as shown in Figures 4a and 5b. At this point, computational efficiency also begins to decline. Considering both computational efficiency and accuracy, the number of elements N in the proposed method is set to 200 for subsequent calculations.

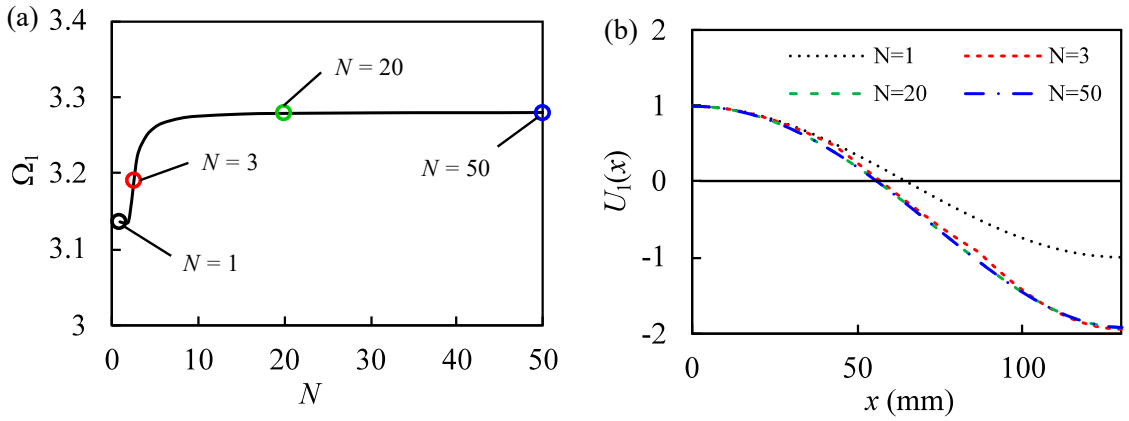


Figure 4. First-order dimensionless natural frequency and its mode shape function for different N: (**a**) Ω_1; (**b**) $U_1(x)$.

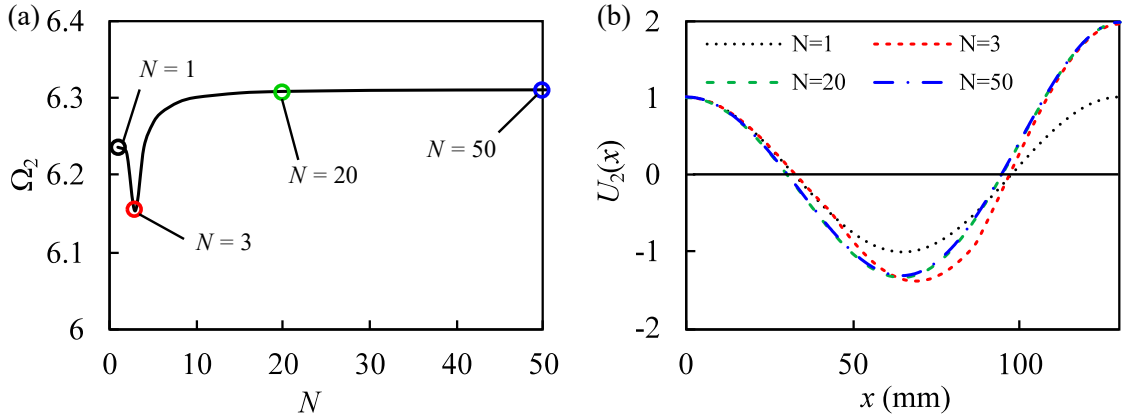


Figure 5. Second-order dimensionless natural frequency and its mode shape function for different N: (**a**) Ω_2; (**b**) $U_2(x)$.

To verify the accuracy of the proposed method, its results were compared with the first five-order dimensionless natural frequencies reported in the literature. Building upon the original calculation examples, the variable c_r was introduced to broaden the comparison scope, defined as $c_r = R_2/R_1$. Additionally, FEM computational results were incorporated into the comparison. The FEM employed SOLID5 element type with 11,520 elements, utilizing a mapped mesh partitioning scheme. Modal analysis was conducted using the Block Lanczos method, while subsequent harmonic response analysis employed the full method. These FEM results were normalized using Equation (47) and are listed alongside the previously dimensionless natural frequencies in Table 2.

As shown in the table, both the proposed method and FEM results are lower than those obtained using traditional methods in the literature. The one-dimensional non-uniform rod wave equation employed by traditional methods does not account for the material's Poisson's ratio. As seen from Equation (13), its stiffness is greater compared to the other two methods, leading to higher calculation results. This deviation increases with higher orders. The proposed method incorporates the Poisson's ratio to account for the lateral inertia effects of non-uniform rods. It treats the one-dimensional stress problem of particles within the rod as an axisymmetric two-dimensional problem, thereby yielding results closer to those of FEM. For rods with uniform cross-sections, the results from both methods are consistent.

Table 2. Comparison of dimensionless natural frequencies for the tapered rod.

Boundary Conditions	c_r	Ω_1	Ω_2	Ω_3	Ω_4	Ω_5
C-F	0.1	2.832	5.691	8.575	11.45	14.29
		2.836 [a]	5.717 [a]	8.659 [a]	11.65 [a]	14.69 [a]
		2.812 [b]	5.652 [b]	8.508 [b]	11.33 [b]	14.01 [b]
	0.5	2.027	4.889	7.878	10.82	13.66
		2.029 [a]	4.913 [a]	7.979 [a]	11.09 [a]	14.21 [a]
		2.022 [b]	4.876 [b]	7.849 [b]	10.73 [b]	13.38 [b]
	1	1.570	4.677	7.694	10.57	13.26
		1.571 [a]	4.712 [a]	7.854 [a]	11.00 [a]	14.14 [a]
		1.570 [b]	4.677 [b]	7.670 [b]	10.41 [b]	12.68 [b]
F-F	0.1	4.061	7.019	9.941	12.83	15.65
		4.070 [a]	7.062 [a]	10.07 [a]	13.10 [a]	16.16 [a]
		4.041 [b]	6.983 [b]	9.878 [b]	12.68 [b]	15.36 [b]
	0.5	3.279	6.310	9.312	12.22	15.01
		3.286 [a]	6.361 [a]	9.477 [a]	12.61 [a]	15.74 [a]
		3.274 [b]	6.300 [b]	9.278 [b]	12.09 [b]	14.54 [b]
	1	3.131	6.200	9.152	11.94	14.53
		3.142 [a]	6.283 [a]	9.425 [a]	12.57 [a]	15.71 [a]
		3.131 [b]	6.194 [b]	9.084 [b]	11.62 [b]	13.59 [b]

Note: C and F denote Fixed and Free boundaries, respectively; [a] indicates data sourced from literature [23]; [b] indicates results calculated by FEM.

To further validate the computational accuracy of the proposed method, comparisons were conducted between the proposed method and FEM results under the following conditions: a small-end radius of 8 mm for the non-uniform rod, an ultrasonic excitation frequency of 20 kHz, both ends free, and a displacement amplitude of 10 μm at the large end. These comparisons were performed at their respective resonant lengths, with FEM results extracted along the axis of the non-uniform rod. When the ultrasonic excitation frequency corresponds to the first natural frequency of longitudinal vibration in the non-uniform rod, the calculated rod lengths obtained by the proposed method and FEM were 129.3 mm and 129.1 mm, respectively, with a relative deviation of less than 0.16%. Similarly, the second natural resonance lengths calculated by these two methods were 250.25 mm and 250.2 mm, respectively, with a relative deviation of less than 0.02%. The close agreement of these results across different orders validates the accuracy of the proposed method. The displacement amplitude distributions and stress amplitude distributions obtained by both methods at the previously resonant lengths are shown in Figures 6 and 7.

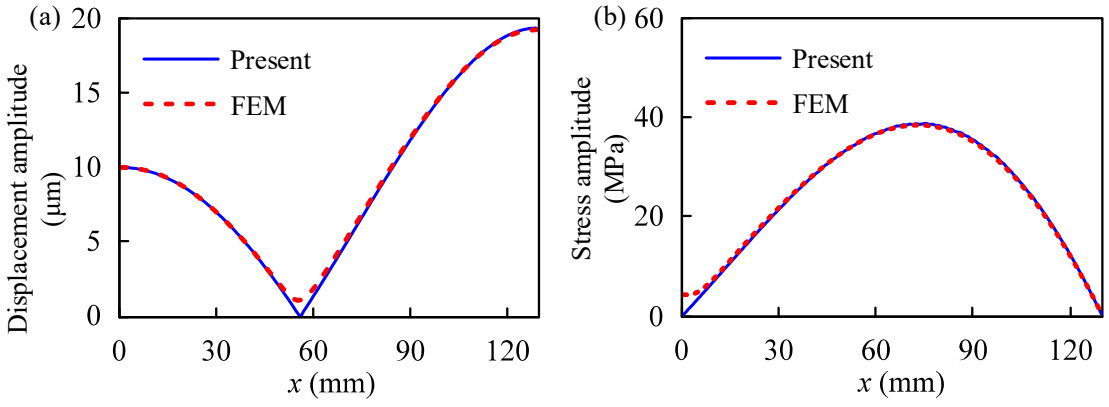


Figure 6. Displacement amplitude/stress amplitude distribution of the non-uniform rod at the first natural frequency: (**a**) Displacement amplitude; (**b**) Stress amplitude.

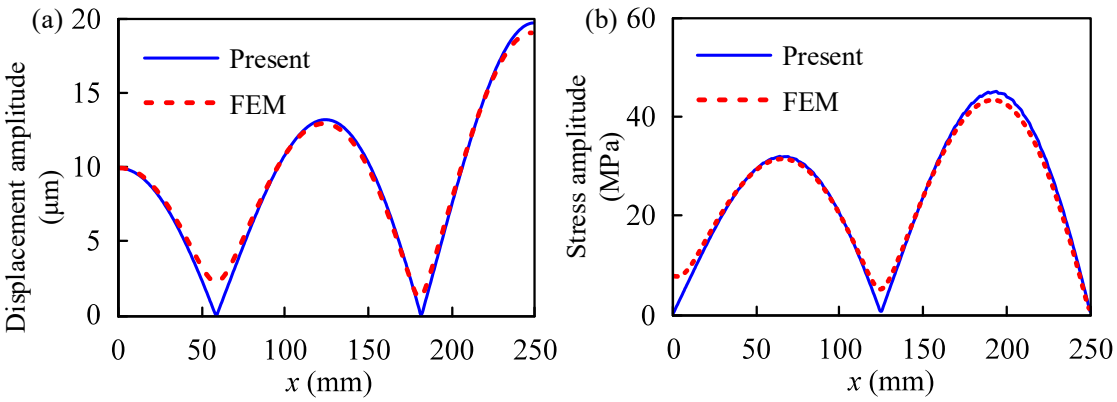


Figure 7. Displacement amplitude/stress amplitude distribution of the non-uniform rod at the second natural frequency: (**a**) Displacement amplitude; (**b**) Stress amplitude.

The curves in Figures 6 and 7 indicate that the computational results of the proposed method show good agreement with the harmonic response analysis results from FEM, particularly at the first natural frequency where the two methods are essentially consistent. In Figure 6a, the node coordinates and maximum displacement amplitudes calculated by both methods are nearly identical, with values of 19.32 μm and 19.21 μm respectively. The difference lies in the residual displacement amplitude at the node observed in the FEM results. This occurs because the proposed method assumes a flat cross-section for the beam, whereas the three-dimensional solid calculation in FEM cannot maintain a flat cross-section due to uneven lateral stress distribution, leading to residual displacement amplitude at the node. Furthermore, the maximum stress amplitude and its axial coordinate calculated by the proposed method in Figure 6b also closely match the FEM results, with maximum stress amplitudes of 38.78 MPa and 38.46 MPa, respectively. This consistency in steady-state response results further validates the accuracy of the model and the computational method established in this paper.

5.2. Application: Ultrasonic Fatigue Specimen

Ultrasonic fatigue specimens typically feature a dumbbell-shaped structure, with dimensions as shown in Figure 8. The figure also indicates the specimen's vibration boundary conditions and the transfer matrices for each section. To facilitate the subsequent introduction of the model and computational methods developed in this paper, an approximate segmented treatment for the variable cross-section portion of the specimen is also illustrated.

The transfer matrix for the non-uniform segment near the excitation end of the ultrasonic fatigue specimen is:

$$\mathbf{T}_{01} = \prod_{i=1}^{N} \mathbf{\Gamma}_{1,i}(L_0/N)\mathbf{\Gamma}_{1,i}^{-1}(0) \tag{48}$$

For definitions of the relevant parameters in this equation, refer to Section 3 of this paper. The difference lies in providing the expressions for the non-uniform segment and radius of the i-th element:

$$S_{1,i} = \pi R_{1,i}^2 \tag{49a}$$

$$R_{1,i} = R_1 + R_0 - \sqrt{R_0^2 - \left(L_0 - \frac{2i-1}{2N}L_0\right)^2} \tag{49b}$$

Similarly, the transfer matrix for the non-uniform segment at the other end of the specimen can be obtained as follows:

$$\mathbf{T}_{02} = \prod_{i=1}^{N} \mathbf{\Gamma}_{2,i}(L_0/N)\mathbf{\Gamma}_{2,i}^{-1}(0) \tag{50}$$

The definitions of related parameters are consistent with those for $\mathbf{T}_{01}$, except that the expression for the cross-sectional radius of the i-th element is different:

$$R_{2,i} = R_1 + R_0 - \sqrt{R_0^2 - \left(\frac{2i-1}{2N} L_0\right)^2} \tag{51}$$

The overall transfer matrix of the ultrasonic specimen can be expressed as:

$$\mathbf{G}_\mathrm{T} = \mathbf{T}_2\mathbf{T}_{01}\mathbf{T}_1\mathbf{T}_{02}\mathbf{T}_2 = \begin{bmatrix} g_{\mathrm{T},11} & g_{\mathrm{T},12} \\ g_{\mathrm{T},21} & g_{\mathrm{T},22} \end{bmatrix} \tag{52}$$

where the expressions for the resonant section transfer matrix $\mathbf{T}_2$ and the gauge section transfer matrix $\mathbf{T}_1$ are similar with those for the element transfer matrices of the non-uniform segments. Using the obtained overall transfer matrix $\mathbf{G}_\mathrm{T}$ and combining it with the boundary conditions shown in Figure 8 (i.e., both ends free), the frequency equation of the specimen is derived from Equation (27):

$$\begin{vmatrix} 0 & 1 \\ g_{\mathrm{T},21} & g_{\mathrm{T},22} \end{vmatrix} = 0 \tag{53}$$

Considering that the loading frequency in ultrasonic fatigue testing is 20 kHz, the first-order natural frequency of the specimen should be the same. The resonant dimension L_2 corresponding to this natural frequency can be solved using the above equation. Then, the natural frequencies and mode shapes for each mode can be further calculated, and the displacement and stress amplitude distributions can be obtained using the modal superposition method.

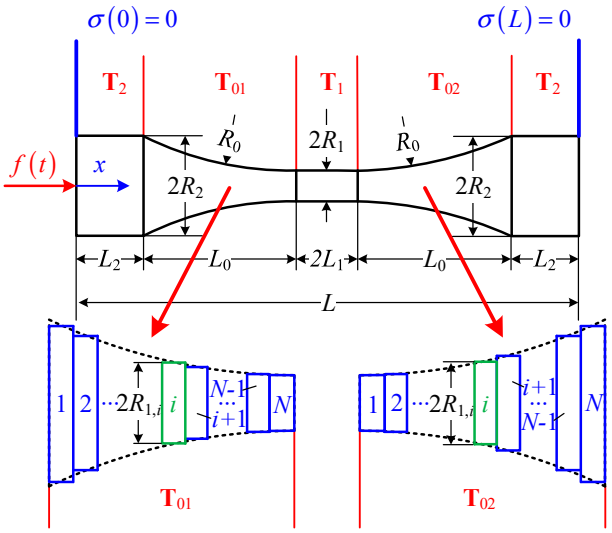


Figure 8. Dimensions of ultrasonic fatigue specimen and Schematic of segmented non-uniform segments.

When the material of the ultrasonic fatigue specimen is TC4 titanium alloy, its parameters are: E = 109 GPa, ρ = 4440 kg/m^3, Poisson's ratio 0.3. Specific specimen dimensions are: R_0 = 40 mm, R_1 = 1.5 mm, R_2 = 5 mm, L_1 = 2 mm. Under ultrasonic excitation (at a frequency of 20 kHz), the constructed model and its computational method yield a resonant dimension L_2 of 9.65 mm, consistent with results obtained using traditional computational method [24]. When applying this calculated value for L_2, commercial FEM software yields a first-order natural frequency of 19,937 Hz for the specimen. This represents a relative deviation of only

0.315% from the expected value (20 kHz), demonstrating the high computational accuracy of the proposed method. Furthermore, commercial FEM(v15.0) software was employed to perform harmonic response analysis on the ultrasonic fatigue specimen. Displacement amplitude and stress amplitude were extracted along the specimen's axis from the analysis results. The extracted FEM results are compared with theoretical calculations as shown in Figure 9.

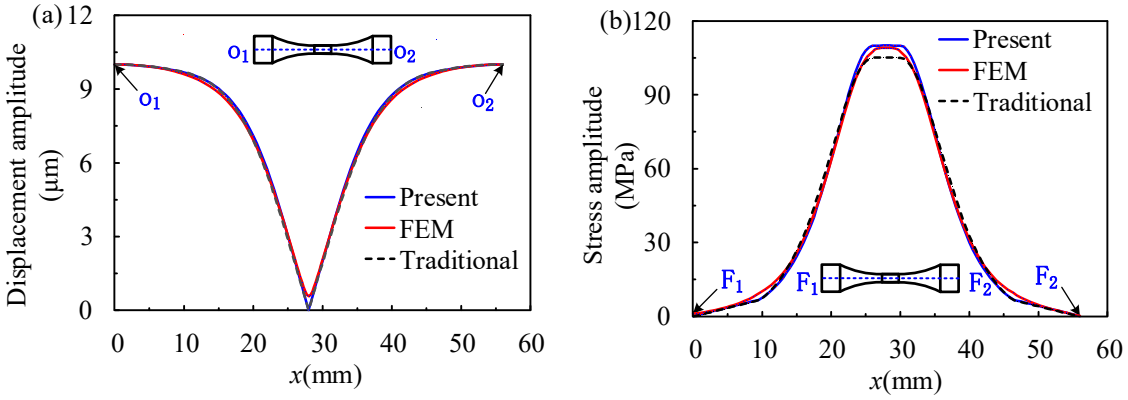


Figure 9. Theoretical and simulation comparison for the ultrasonic fatigue specimen: (**a**) Displacement amplitude; (**b**) Stress amplitude.

The results in the figure indicate that the displacement amplitudes calculated by the three methods are relatively close, but the stress amplitudes show significant differences. The proposed method in this paper is more consistent with the FEM results, especially at the maximum stress point of the specimen, while the traditional method exhibits significant deviations near the gauge section. This discrepancy primarily results from the approximation of the circular arc transition in the specimen as a catenary transition in traditional computational methods, a point also discussed in Reference [8]. Considering that strain gauges cannot monitor the stress level of specimens throughout the entire cycle in ultrasonic fatigue testing, the displacement amplitude at the specimen ends is typically used to monitor the stress amplitude in the gauge section. If the results from the traditional method are used to guide the conversion between the displacement amplitude at the ends and the stress amplitude in the gauge section, it will lead to the stress level in the fatigue test being higher than the target stress level. Therefore, employing the proposed method in this paper for estimating stress levels in ultrasonic fatigue specimens has important practical significance.

6. Conclusions

For the design requirements of non-uniform rods (such as ultrasonic transducers and fatigue specimens) in fields like ultrasonic machining, ultrasonic welding, and ultrasonic fatigue, this paper carries out a vibration analysis research on non-uniform rods under ultrasonic excitation. The primary conclusions are as follows:

1. A vibration model for non-uniform rods under ultrasonic excitation was established, incorporating the influence of lateral inertia. The model also accounts for material damping by introducing the Kelvin model.

2. Based on TMM, a free vibration analysis of non-uniform rod considering lateral inertia effects was conducted, yielding calculation methods for the natural frequencies and mode shape functions of non-uniform rod.

3. A steady-state response analysis of non-uniform rods under ultrasonic excitation was conducted, and the orthogonality conditions for their mode shape functions were derived. Subsequently, the displacement distribution function and stress distribution

function of non-uniform rods under ultrasonic excitation were obtained using the modal superposition method.

4. Typical non-uniform rods (i.e., tapered rods) were used as validation examples to demonstrate the validity and accuracy of the established model and its computational method. Comparisons with traditional methods and FEM revealed that the proposed method produced natural frequencies closer to FEM results for all orders, with both approaches yielding values lower than traditional calculations. This discrepancy is due to the traditional method's failure to account for lateral inertia effects. Furthermore, the resonant lengths calculated by the proposed method and FEM are highly consistent (with a relative deviation of less than 0.16%), and their harmonic response analysis results also show excellent agreement.

5. Ultrasonic fatigue specimens were used as typical application examples to further validate the universality and accuracy of the established model and its computational method. The proposed method yielded the frequency equation for ultrasonic fatigue specimens and provided a design method for their resonant dimensions. The designed specimen was verified via FEM, showing a relative deviation of only 0.315% between its first-order natural frequency and the expected value. Furthermore, compared to traditional computational methods, this paper's proposed method yields displacement amplitude and stress amplitude distribution curves that more similarly match the FEM results, particularly with nearly similar maximum stress values.

With regard to the fact that the subject of this study is a non-uniform rod under ultrasonic excitation, the established model and computational methods are universally applicable. The research results are expected to be applicable to the resonance design and performance evaluation of rod-type longitudinal vibration components in ultrasonic vibration systems.

Nevertheless, it should be noted that while the current model achieves a significant balance between predictive accuracy and computational efficiency, certain limitations regarding specific physical details persist. For instance, due to the inherent constraints of the plane section assumption, the model cannot yet capture non-uniform lateral stress effects. This identified limitation will serve as a critical point of departure for the in-depth optimization of the theoretical model in future investigations.

Author Contributions: Conceptualization, J.W. and Y.Z. (Yuehang Zhang); methodology, J.W.; software, Y.Z. (Yuehang Zhang); validation, J.W. and Y.Z. (Yuehang Zhang); formal analysis, C.C., Q.G. and G.X.; investigation, K.S., Y.M., Q.L. and M.L.; resources, J.W.; data curation, Y.Z. (Yuehang Zhang); writing—original draft preparation, Y.Z. (Yuehang Zhang); writing—review and editing, Y.Z. (Yuehang Zhang); visualization, Y.Z. (Yuehang Zhang); supervision, J.W. and Y.Z. (Yan Zhang); project administration, J.W.; funding acquisition, J.W. All authors have read and agreed to the published version of the manuscript.

Funding: This research was funded by Scientific Research Program of Jilin Provincial Department of Education, grant number JJKH20251094KJ, and the Research Initiation Program for Doctoral Talents at Changchun University, grant number ZKQD202404 and the APC were funded by the Scientific Research Program of Jilin Provincial Department of Education, grant number JJKH20251094KJ.

Data Availability Statement: The original contributions presented in this study are included in the article. Further inquiries can be directed to the corresponding author.

Conflicts of Interest: The authors declare no conflicts of interest.

References

1. Yang, Z.; Zhu, L.; Zhang, G.; Ni, C.; Lin, B. Review of ultrasonic vibration-assisted machining in advanced materials. *Int. J. Mach. Tools Manuf.* **2020**, *156*, 103594. [CrossRef]
2. Roy, S.; Jagadish. Design of a circular hollow ultrasonic horn for USM using finite element analysis. *Int. J. Adv. Manuf. Technol.* **2017**, *93*, 319–328. [CrossRef]
3. Li, X.; Harkness, P.; Worrall, K.; Timoney, R.; Lucas, M. A Parametric Study for the Design of an Optimized Ultrasonic Percussive Planetary Drill Tool. *IEEE Trans. Ultrason. Ferroelectr. Freq. Control* **2017**, *64*, 577–589. [CrossRef] [PubMed]
4. Roopa, R.M.; Prakasan, K.; Rudramoorthy, R. Studies on thermo-elastic heating of horns used in ultrasonic plastic welding. *Ultrasonics* **2015**, *55*, 123–132. [CrossRef] [PubMed]
5. Roopa, R.M.; Rudramoorthy, R. Computational modeling and experimental studies of the dynamic performance of ultrasonic horn profiles used in plastic welding. *Ultrasonics* **2013**, *53*, 763–772. [CrossRef] [PubMed]
6. Cheng, X.M.; Yang, K.; Wang, J.; Xiao, W.; Huang, S. Ultrasonic system and ultrasonic metal welding performance: A status review. *J. Manuf. Process.* **2022**, *84*, 1196–1216. [CrossRef]
7. Zhao, J.C.; Wan, J.; Zhang, S.Z.; Yan, C.; Zhao, H. Application of ultrasonic fatigue technology in very-high-cycle fatigue testing of aviation gas turbine engine blade materials: A review. *Sci. China-Technol. Sci.* **2024**, *67*, 1317–1363. [CrossRef]
8. Myung, N.; Choi, N.-S. Dynamic stress analysis of the specimen gauge portion with a circular profile for the ultrasonic fatigue test. *Int. J. Fatigue* **2016**, *92*, 71–77. [CrossRef]
9. Paolino, D.; Tridello, A.; Chiandussi, G.; Rossetto, M. On specimen design for size effect evaluation in ultrasonic gigacycle fatigue testing. *Fatigue Fract. Eng. Mater. Struct.* **2014**, *37*, 570–579. [CrossRef]
10. Bathias, C.; Paris, P.C. *Gigacycle Fatigue in Mechanical Practice*; CRC Press: New York, NY, USA, 2004.
11. Lin, Z.M. *The Principle and Design of Ultrasonic Horns*; Science Press: Beijing, China, 1987.
12. Lesniewski, P. Discrete component equivalent circuit for Webster's horns. *Appl. Acoust.* **1995**, *44*, 117–124. [CrossRef]
13. Yang, J.; Fang, Z.; Wei, B.; Deng, X. Theoretical explanation of the 'local resonance' in stepped acoustic horn based on Four-End Network method. *J. Mater. Process Technol.* **2009**, *209*, 3106–3110. [CrossRef]
14. Qu, D.G.; Xiang, D.; Mou, P. Design of the ultrasonic atomizing nozzle's vibration system based on a piecewise approximate method. *J. Mech. Eng.* **2012**, *48*, 10. [CrossRef]
15. Mori, E.; Itoh, K.; Imamura, A. Analysis of a short colum vibrator by apparent elasticity method and its application. *Proc. Ultrason. Int.* **1977**, 262–266.
16. Lin, S.Y.; Zhang, F.C. Research on lateral vibration in power ultrasonic vibration systems. *J. Shaanxi Norm. Univ.* **1993**, 41–43. [CrossRef]
17. Yazdian, A.; Karafi, M.R. An analytical approach to design horns and boosters of ultrasonic welding machines. *SN Appl. Sci.* **2022**, *4*, 166. [CrossRef]
18. Pestel, E.; Leckie, F.A. *Matrix Methods in Elastomechanics*; McGraw-Hill: New York, NY, USA, 1963.
19. Wang, L.L. *Foundation of Stress Waves*, 2nd ed.; National Defense Industry Press: Beijing, China, 2005.
20. Gallego-Juárez, J.A.; Graff, K.F. *Power Ultrasonics: Applications of High-Intensity Ultrasound*; Woodhead Publishing: Oxford, UK, 2014.
21. de Silva, C.W. *Vibration Damping, Control, and Design*; CRC Press: Boca Raton, FL, USA, 2007.
22. Hu, H.Y. *Fundamentals of Mechanical Vibration*; Beihang University Press: Beijing, China, 2005.
23. Yang, Y.-B.; Kang, J.-H. Closed-form exact solutions for hysteretically damped longitudinal free and forced vibrations of tapered beams. *Acta Mech.* **2018**, *229*, 4741–4751. [CrossRef]
24. Green, C.H. The ultrasonic stress distribution in the fatigue dumb-bell specimen. *J. Phys. D Appl. Phys.* **1981**, *14*, 1551–1559. [CrossRef]

Disclaimer/Publisher's Note: The statements, opinions and data contained in all publications are solely those of the individual author(s) and contributor(s) and not of MDPI and/or the editor(s). MDPI and/or the editor(s) disclaim responsibility for any injury to people or property resulting from any ideas, methods, instructions or products referred to in the content.